Paper No.
13157

NACE INTERNATIONAL CORROSION Conference & Expo 2019

Development of a Prediction Model for High pCO_2 Corrosion of Mild Steel

Yoon-Seok Choi, Shokrollah Hassani, Thanh Nam Vu, Srdjan Nesic
Institute for Corrosion and Multiphase Technology,
Department of Chemical and Biomolecular Engineering, Ohio University
342 West State Street
Athens, OH 45701
USA

Ahmad Zaki B Abas, Azmi Mohammed Nor, Muhammad Firdaus Suhor
PETRONAS Research SDN. BHD, Selangor Darul Ehsan, Malaysia

ABSTRACT

Most of the corrosion prediction models used for design of oil and gas lines carrying high pCO_2 are valid up to 1 ~ 2 MPa of pCO_2 and are very conservative at higher pCO_2 because they do not account for the effect of high pCO_2 on the water chemistry and the corrosion mechanism. The present work was focused on developing a predictive tool for near-critical and supercritical CO_2 corrosion of mild steel. It incorporates changes in the water chemistry module due to update solubility and dissociation equations, changes in the electrochemical module due to the presence of a thick and porous corrosion product layer, and consideration of an adsorption mechanism for H_2CO_3 at the steel surface. The comparison between experimental results and model predictions showed a good agreement under various pressure and temperature ranges.

Key words: Supercritical CO_2, CO_2 corrosion, carbon steel, corrosion model

INTRODUCTION

Internal corrosion of carbon steel pipeline in high partial pressure CO_2 (pCO_2) environments have gained more interest recently relating to carbon capture and storage (CCS), enhanced oil recovery (EOR), and deep water oil and gas production applications.[1-5] Although there are extensive research data available on high pCO_2 corrosion, minimal information has been reported in the literature that could aid in

establishing a corrosion model for carbon steel in such conditions.[6-8] Furthermore, the published literature on supercritical CO_2 primarily addresses topics related to sequestration and enhanced oil recovery (EOR) that usually involve "dry" gases where water is only present at the ppm level.

The impact of aqueous CO_2 corrosion on carbon steel has been studied extensively at pressures relevant for oil and gas transport (up to 2 MPa CO_2). Therefore, most of the predictive models used for design of oil and gas lines carrying high pCO_2 are valid up to 1 ~ 2 MPa of pCO_2 and are very conservative at higher pCO_2.[9-12]

It has been reported that aqueous corrosion mechanisms in high pCO_2 are similar to those in low pCO_2 conditions including characteristics of corrosion product layer and the response of corrosion rate with temperature.[13] This indicates that the existing CO_2 corrosion model could be used to predict the corrosion rate at high pCO_2 conditions with some modifications in chemical, electrochemical or transport processes. For example, since CO_2 changes from gaseous to liquid or supercritical with increasing pressure, it will lead to different interaction with water, i.e. CO_2 solubility in water will not follow Henry's law in liquid or supercritical CO_2 conditions, which results in changing water chemistry.[14]

Thus, the objective of the present study was to develop a predictive model for high pCO_2 corrosion of mild steel considering with changes in chemical and electrochemical reactions.

MODEL DESCRIPTION

The mechanistic model developed by Nesic et al., in early 2000 covers most of the key processes present in uniform CO_2 corrosion of carbon steel: electrochemical reactions at the steel surface, chemical reactions and transport of species between the steel surface and the bulk solution, and formation/growth of iron carbonate ($FeCO_3$) layer. The physical, mathematical, and numerical aspects of the model are explained in detail in the previous papers.[15-18] In the present study, this model was used as a base platform and the key aspects of the model are briefly described below:

Water Chemistry Model

Understanding water chemistry is an important precondition for predicting CO_2 corrosion of carbon steel. Various chemical reactions take place in the water phase due to the presence of CO_2. For a CO_2 aqueous system, the following reactions are taken into consideration at all times:

$$CO_{2(g)} \overset{Ksol}{\longleftrightarrow} CO_{2(aq)} \quad \text{(Dissolution of } CO_2\text{)} \tag{1}$$

$$CO_{2(aq)} + H_2O \overset{Khyd}{\longleftrightarrow} H_2CO_3 \quad \text{(Hydration of aqueous } CO_2\text{)} \tag{2}$$

$$H_2CO_3 \overset{Kca}{\longleftrightarrow} H^+ + HCO_3^- \quad \text{(Dissociation of carbonic acid)} \tag{3}$$

$$HCO_3^- \overset{Kbi}{\longleftrightarrow} H^+ + CO_3^{2-} \quad \text{(Dissociation of bicarbonate ion)} \tag{4}$$

$$H_2O \overset{Kw}{\longleftrightarrow} H^+ + OH^- \quad \text{(Dissociation of water)} \tag{5}$$

The reactions shown above can be described by equilibria reactions as follows based on the assumption of infinite dilution:

$$K_{sol} = \frac{C_{CO_{2(aq)}}}{P_{CO_{2(g)}}} \tag{6}$$

$$K_{hyd} = \frac{C_{H_2CO_3}}{C_{CO_2}\, C_{H_2O}} \tag{7}$$

$$K_{ca} = \frac{C_{H^+}\, C_{HCO_3^-}}{C_{H_2CO_3}} \tag{8}$$

$$K_{bi}=\frac{C_{H^+}\,C_{CO_3^{2-}}}{C_{HCO_3^-}} \quad (9)$$

$$K_w=\frac{C_{H^+}\,C_{OH^-}}{C_{H_2O}} \quad (10)$$

where C_{CO_2}, $C_{H_2CO_3}$, $C_{HCO_3^-}$, $C_{CO_3^{2-}}$, C_{H^+}, and C_{OH^-} are the concentrations (mol/L) of CO_2, carbonic acid, bicarbonate ion, carbonate ion, hydrogen ion, and hydroxide ion, respectively.

The equilibrium constants, K, are a function of the temperature and are available in the open literature. Since the solution cannot have a net charge, an electroneutrality relation is required. Mathematically, it is expressed:

$$C_{H^+} = C_{HCO_3^-}+2\times C_{CO_3^{2-}}+C_{OH^-} \quad (11)$$

<u>Electrochemical Model</u>

As the CO_2 corrosion process is electrochemical in nature, the corrosion rate can be explicitly determined by calculating the rate of the electrochemical reactions occurring simultaneously at the steel surface:

Anodic (oxidation) reaction:

$$Fe \rightarrow Fe^{2+} + 2e- \quad (12)$$

Cathodic (reduction) reactions:

$$H^+ + e^- \rightarrow \tfrac{1}{2}H_2 \quad (13)$$

$$H_2CO_3 + e^- \rightarrow \tfrac{1}{2}H_2 + HCO_3^- \quad (14)$$

The electrochemical reaction rate can be expressed as a current density, *i* (expressed in $A\ m^{-2}$), which is a function of the potential at the metal surface, *E* (expressed in *V)*:

$$i=\pm i_0\times 10^{\pm\frac{E-E_{rev}}{b}}\times \prod_{s=1}^{n_s}(1-\theta_s) \quad (15)$$

This equation is unique for each of the electrochemical reactions involved in a corrosion process such as iron oxidation, hydrogen reduction and carbonic acid reduction. The "+" sign applies for anodic reactions while the "-" sign applies for cathodic reactions. θ_s is the fraction of the steel surface where a given electrochemical reaction does not occur because the surface is covered by a species *s* which could be an adsorbed inhibitor or a protective film. The product sign $\prod$ accounts for a compounding (additive) effect by more than one surface species. For each electrochemical reaction, Equation (1) is different because of the parameters defining it: i_0 - the exchange current density in $A\ m^{-2}$, E_{rev} - the reversible potential in *V*, and *b* – the Tafel slope in *V*. These parameters have to be determined experimentally and are functions of temperature and in some cases species concentrations. The unknown potential at the metal surface *E* in Equation (15), is also called the corrosion potential or open circuit potential, which can be found from the charge balance equation at the metal surface:

$$\sum_{a=1}^{n_a} i_a = \sum_{c=1}^{n_c} i_c \quad (16)$$

where n_a and n_c are the total number of anodic and cathodic reactions respectively.

<u>$FeCO_3$ Layer Formation and Growth Model</u>

Solid $FeCO_3$ forms when the concentrations of Fe^{2+} and CO_3^{2-} exceed the solubility limit according to the following reaction:

$$Fe^{2+}_{(aq)} + CO_3^{2-}{}_{(aq)} \leftrightarrow FeCO_{3(s)} \quad (17)$$

When $FeCO_3$ precipitates on the steel surface, it can slow down the corrosion process not only by presenting a diffusion barrier for the species involved in the corrosion process but also by blocking a portion of the steel surface and preventing the underlying steel from further corrosion.

The governing equation for $FeCO_3$ layer growth based on mass conservation of $FeCO_3$ in the solution is shown in equation (18).

$$\frac{\partial \varepsilon}{\partial t} = -\frac{M_{FeCO_3}}{\rho_{FeCO_3}} \frac{A}{V} R_{FeCO_3} - CR \frac{\partial \varepsilon}{\partial x} \quad (18)$$

where ε is porosity, t is time, M_{FeCO_3} is molar mass of $FeCO_3$, ρ_{FeCO_3} is density of $FeCO_3$, $\frac{A}{V}$ is area-volume ratio, R_{FeCO_3} is precipitation rate of $FeCO_3$, CR is corrosion rate, and x is distance. In this equation, $FeCO_3$ layer growth is characterized by the change in porosity (ε), which changes between 0 and 1. A value of 1 indicates that no $FeCO_3$ layer forms while a value of 0 represents that the surface is completely filled with $FeCO_3$. This equation suggests that the growth of $FeCO_3$ layer is attributed to two factors: $FeCO_3$ precipitation and undermining steel corrosion. Depending on the relative values of these two terms, $FeCO_3$ layer can be either protective or non-protective.

RESULTS AND DISCUSSION

Modification in Water Chemistry Model

In low pCO_2 system, the concentration of dissolved CO_2 in water is directly proportional to its partial pressure (Equation 1). The solubility constant is calculated and derived using Henry's constant (K_{sol}) as the concentration of dissolved CO_2 is relatively small. In high pCO_2 systems, however, the relationship between concentration and pressure is not linear and Henry's law cannot be used directly. Instead, the non-ideality of the CO_2 phase must be taken into account. In the present study, two different CO_2 solubility models were selected from open literature for high pCO_2 conditions[19-21] and compared with the case with Henry's law. Figure 1 shows the comparison of mole fraction of CO_2 in water as a function of pCO_2 calculated from different solubility models at 25°C and 60°C. It shows that the amount of dissolved CO_2 increased with increasing pCO_2. It can be also seen that as pCO_2 increases, the solubility of CO_2 in water deviates further from Henry's Law; that is, the domain of validity of Henry's Law is at best 2 MPa at 25°C, and only 0.8 MPa at 60°C.[22] In addition, there is no significant difference in CO_2 content between the high pCO_2 solubility models.

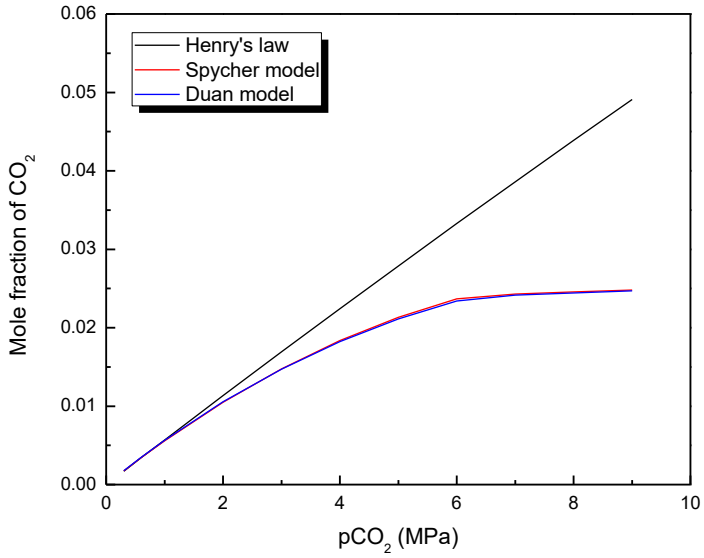

(a)

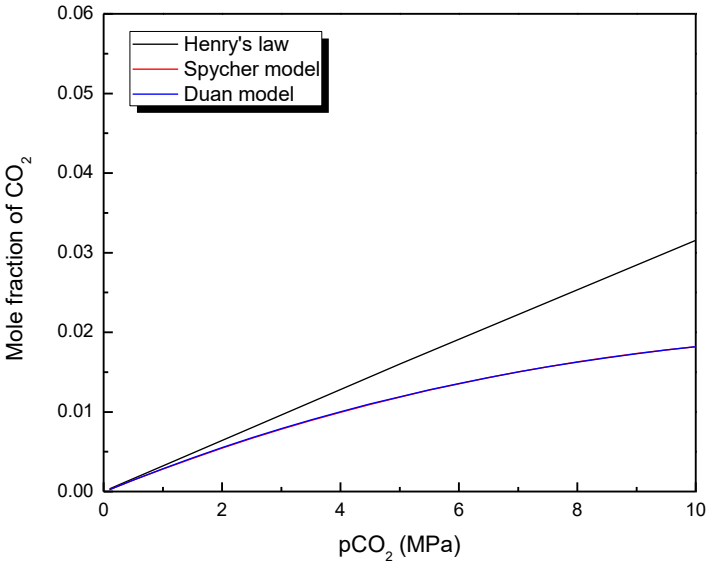

(b)

Figure 1: Comparison of the calculated molar fraction of dissolved CO_2 in water based on Henry's law and high pCO_2 solubility models as a function of pCO_2: (a) 25ºC, (b) 60ºC.

Other equilibrium constants were also compared between low pCO_2 and high pCO_2 models. For example, the equilibrium constant for carbonic acid dissociation (K_{ca}) is calculated in the low pCO_2 model as:[15]

$$K_{ca} = 387.6 \times 10^{-(6.41-1.594\times10^{-3}T_f+8.52\times10^{-6}T_f^2-3.07\times10^{-5}p-0.4772\times I^{\frac{1}{2}}+0.118\times I)} \quad (19)$$

where T_f is the temperature in degrees Fahrenheit, p is the pressure in psi and I is the ionic strength in molar. For the high pCO_2 model, K_{ca} was taken from open literature that can cover the temperature range of 0ºC to 100ºC and the pressure range of 0.1 to 300 MPa:[23,24]

$$\begin{aligned}\ln K_{ca} = {} & 233.5159304 - 11974.38348T^{-1} - 36.50633536\ln T \\ & +(-45.08004597T^{-1} + 2131.318848T^{-2} + 6.714256299T^{-1}\ln T)(P - P_s) \\ & +(0.008393915212T^{-1} - 0.4015441404T^{-2} - 0.00124018735T^{-1})(P - P_s)^2 \end{aligned} \quad (20)$$

where P_s is the saturation pressure of water, P is the CO_2 pressure in bar, and T is the temperature in Kelvin. Figure 2 compares the pK_{ca} values as a function of pCO_2 calculated by Equation 16 and Equation 17 at 25°C and 60°C. Although the pK_{ca} of high pCO_2 model was slightly higher than that of low pCO_2 model, it will not cause a significant difference in the calculation of species concentrations. The same trend was observed for the comparison of other equilibrium constants between low pCO_2 model and high pCO_2 model.

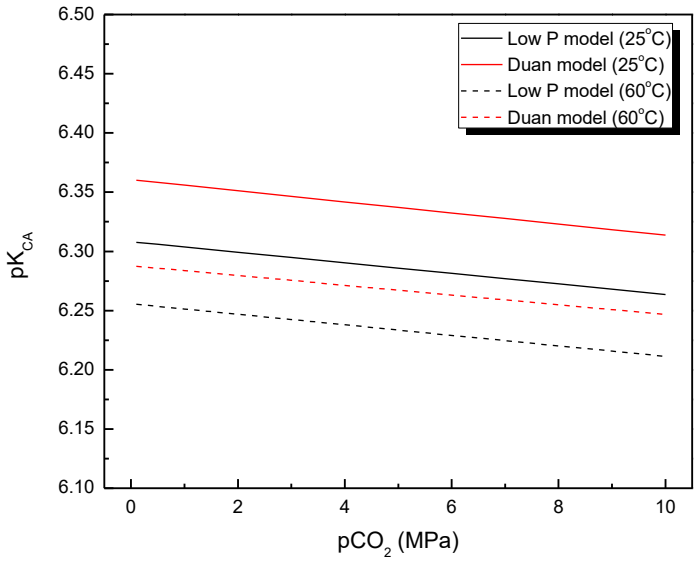

Figure 2: Comparison of the pK_{ca} calculated by low pCO_2 model and high pCO_2 model as a function of pCO_2 at 25°C and 60°C.

Figure 3 shows the pH values as a function of pCO_2 calculated by low pCO_2 model and high pCO_2 model at 25°C and 60°C. The pH values decreased with increasing pCO_2 due to the increase of the dissolved CO_2 amount (Figure 1). However, a significant effect of non-ideal behavior of CO_2 at high pressures on the pH can be seen due to the deviation from the solubility calculations based on Henry's law and the high pCO_2 solubility model. This result suggests that utilizing the low pCO_2 water chemistry model could overestimate the corrosion rate in high pCO_2 conditions due to the inaccurate prediction of pH.

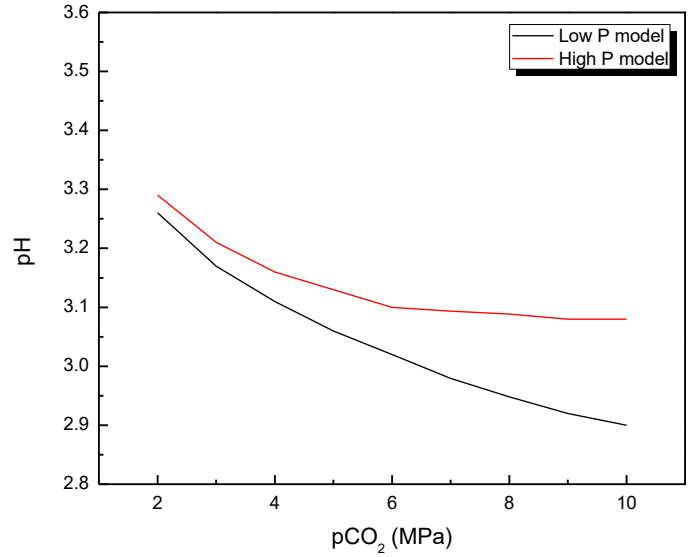

(a)

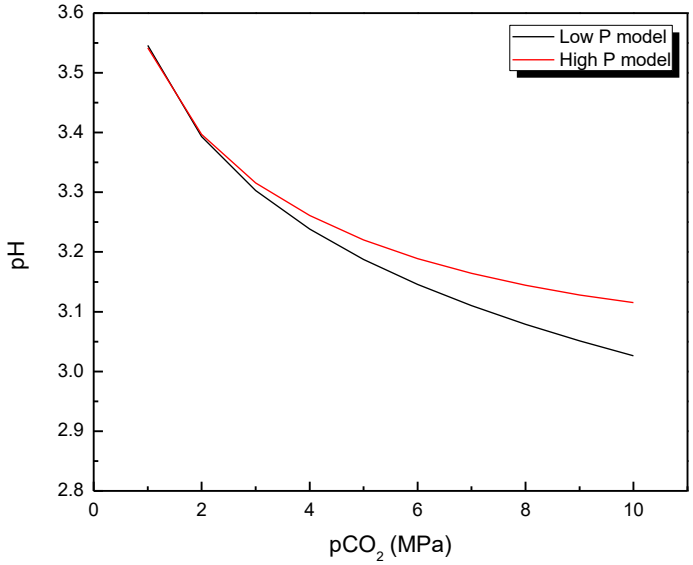

(b)

Figure 3: Comparison of the calculated solution pH based on low pCO_2 model and high pCO_2 model as a function of pCO_2: (a) 25°C, (b) 60°C.

Modification in Electrochemical Model

The modified water chemistry model was implemented and the corrosion rate was predicted in conjunction with the original electrochemical model. However, the corrosion rates were still over-predicted as compared to experimental data by a factor of 2 to 4.

If the species concentrations are predicted correctly with the high pCO_2 water chemistry model, then the over prediction of corrosion rates may be a result of not considering the limited ability for the corrosive species to adsorb on the steel surface in order to be reduced. In other words, it can be assumed that all the increased concentrations of species, such as H^+ and H_2CO_3 due to the increase in pCO_2 can not adsorb to the metal surface due to the reaction site limitations. Therefore, the cathodic reduction reactions become limited by adsorption kinetics resulting in plateau for the corrosion rate at high pCO_2 conditions. This phenomenon was implemented using a Langmuir adsorption isotherm:

$$\theta = 1 - \frac{K.pCO_2}{1+K.pCO_2} \quad (21)$$

where θ is the fractional surface coverage for species at the steel surface, and *K* is the adsorption equilibrium constant. The value of θ determines availability of the reducible species at the surface. Figure 4 shows the fractional surface coverage coefficient as a function of pCO_2.

Since H_2CO_3 is by far the main cathodic species in the corrosion reaction at high pCO_2 conditions (as compared to H^+), the implementation of the adsorption coefficient Θ has been applied to the calculation of the current density of H_2CO_3 reduction reaction. This will reduce the influence of H_2CO_3 on the corrosion behavior and consequently dampen the corrosion rates at high pCO_2 conditions.

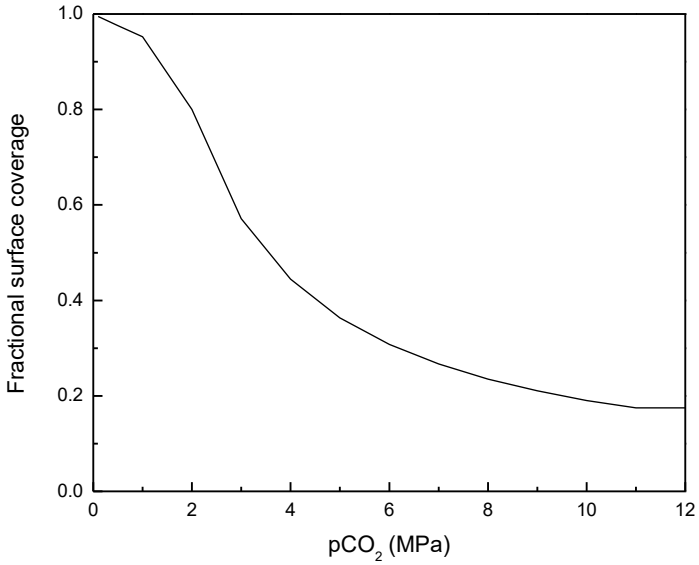

Figure 4: Fractional surface coverage coefficient as a function of pCO_2.

Modification in $FeCO_3$ Layer Formation and Growth Model

Solving equation (15) accounts several numerical issues. For example, the first term on the right hand side (RHS) of equation (15) is a hyperbolic equation with stiff non-linear source term. Furthermore, the second term on the RHS of equation (15) poses a convective-like effect in the equation. A convective term contributes to numerical instability in solving a partial differential equation, which includes incorrect front propagation and severe limit on time step. The numerical instability is more pronounced at high pCO_2 conditions. Thus in the present study, to minimize numerical instability, the hyperbolic precipitation rate equation was solved implicitly using exact analytical solution and front tracking scheme ($\varepsilon_{i,j}^{n+1} = \varepsilon_{i,j-1}^{n}$)was implemented for the convective component.

Equation (15) is solved in the 1D domain as shown in Figure 5. At the $FeCO_3$ layer/metal surface interface, the porosity is considered to be 1, as the corrosion process continuously creates voids underneath the $FeCO_3$ layer. At the other boundary (between the diffusion boundary layer and the bulk solution), it is assumed that no $FeCO_3$ can grow onto the boundary and out of the domain; therefore, porosity of $FeCO_3$ maintains at 1.

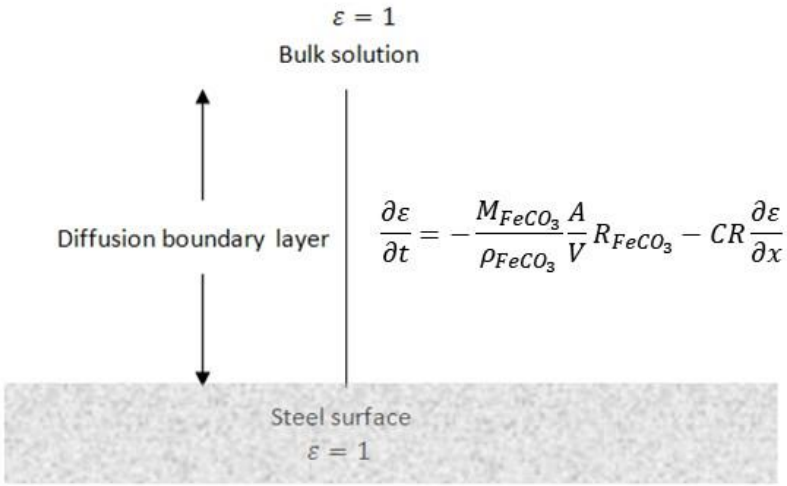

Figure 5: Computation domain and governing equation for $FeCO_3$ layer growth simulation.

Parametric Study

Figure 6 shows the effect of pCO_2 on corrosion rate from model prediction for different pH values at 80°C. It is seen that the corrosion rate increases with increasing pCO_2 for both pH values. Figure 7 shows the effect of temperature on corrosion rate at 12 MPa of pCO_2. The corrosion rate increases with the increase in temperature due to the higher reaction rate at higher temperature. It is also observed that the corrosion rate changed greatly from 50°C to 80°C. Figure 8 represents the effect of pH on corrosion rate at 12 MPa of pCO_2 and 80°C. The corrosion rate slightly decreases from pH 3 to 5 and then it decreases to very low corrosion rate at pH 6 due to the formation of protective $FeCO_3$. Figure 9 shows the effect of flow velocity on corrosion rate for different temperatures at 12 MPa of pCO_2 and pH 3. It is observed that the increase in flow velocity accelerates the corrosion reaction at higher temperature (80°C).

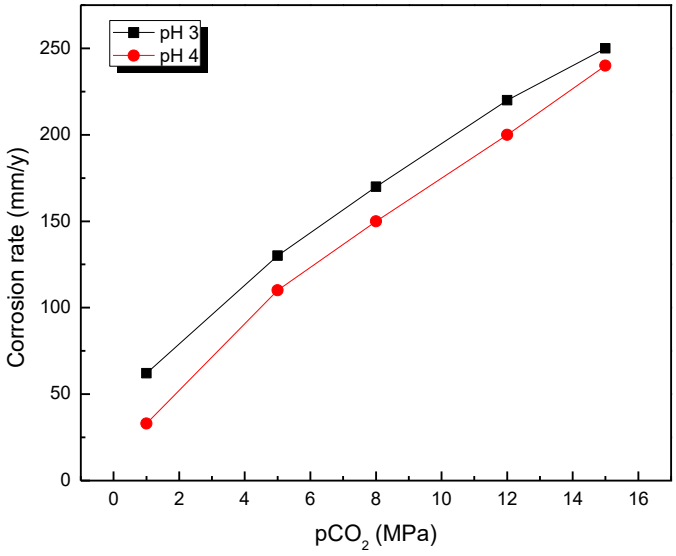

Figure 6: Effect of pCO_2 on corrosion rate at different pH values (80°C and 1 m/s flow velocity).

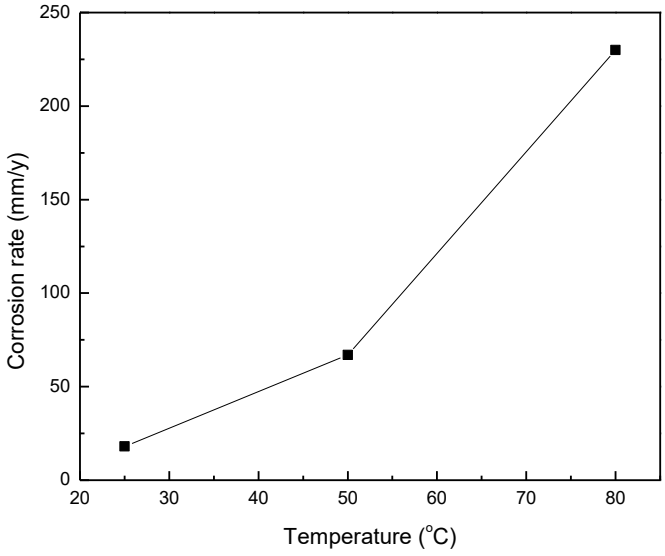

Figure 7: Effect of temperature on corrosion rate at pH 3 (12 MPa pCO_2 and 1 m/s flow velocity).

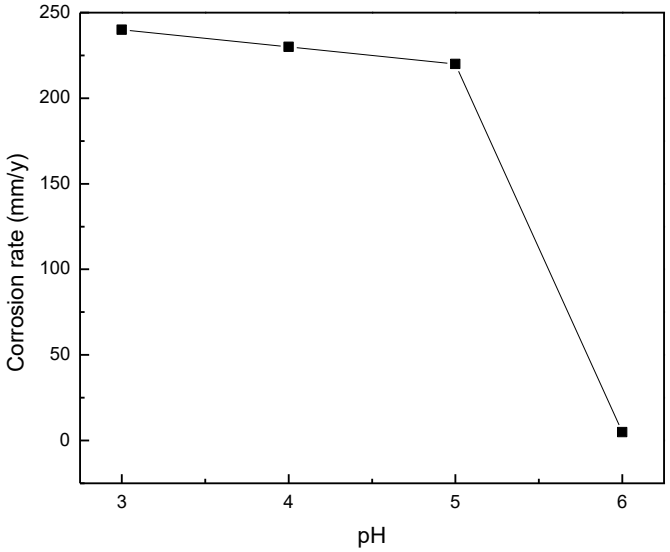

Figure 8: Effect of pH on corrosion rate at 80°C (12 MPa pCO_2 and 1 m/s flow velocity).

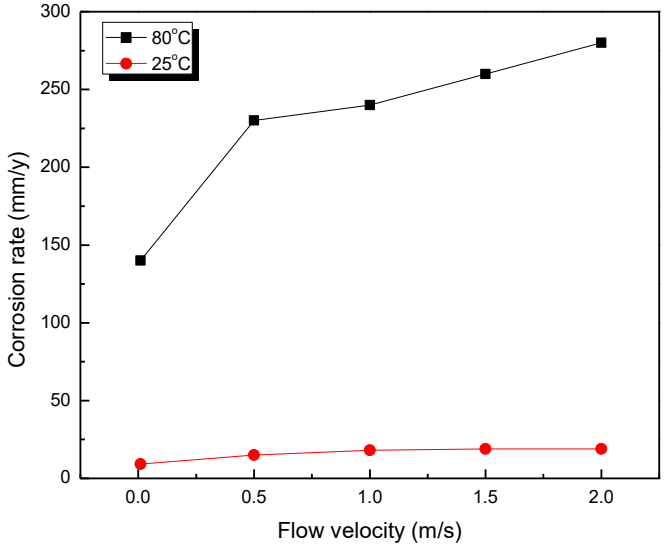

Figure 9: Effect of flow velocity on corrosion rate at different temperatures (12 MPa pCO_2 and pH 3).

Model Validation

The comparison between experimental data (obtained from autoclave and high pressure flow loop experiments)[25-27] and model prediction is shown in Figure 10 under different combinations of pressure and temperature. The predicted corrosion rates show a good agreement with experimental data. Many similar comparisons were made for other conditions covered in this study, with similar results.

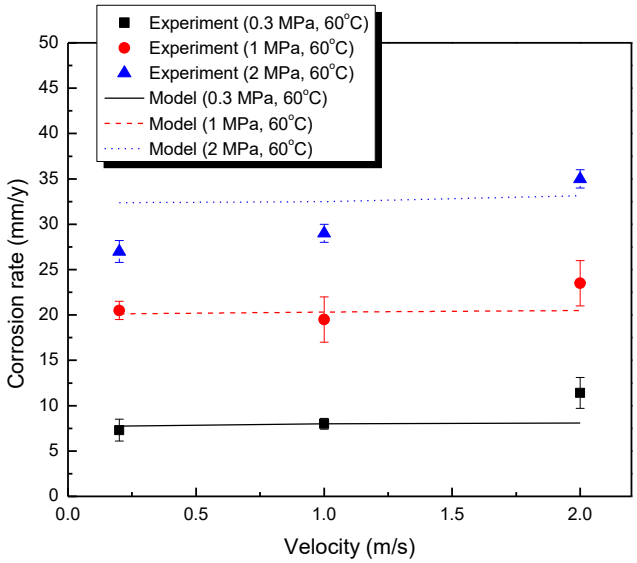

(a)

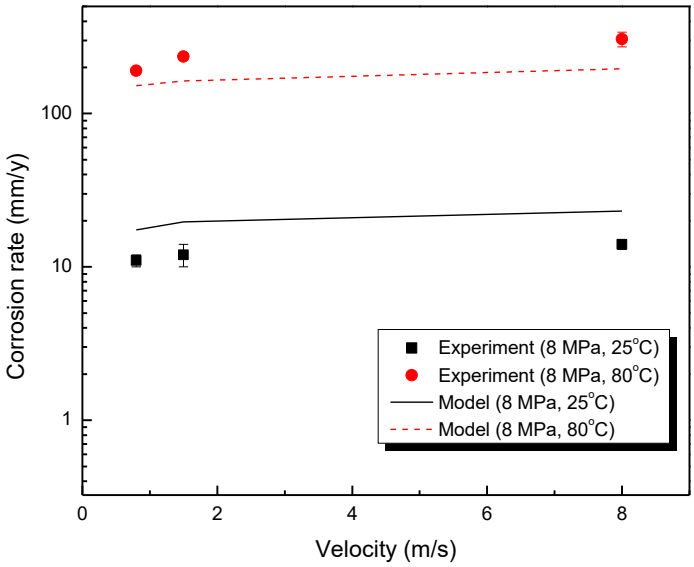

(b)

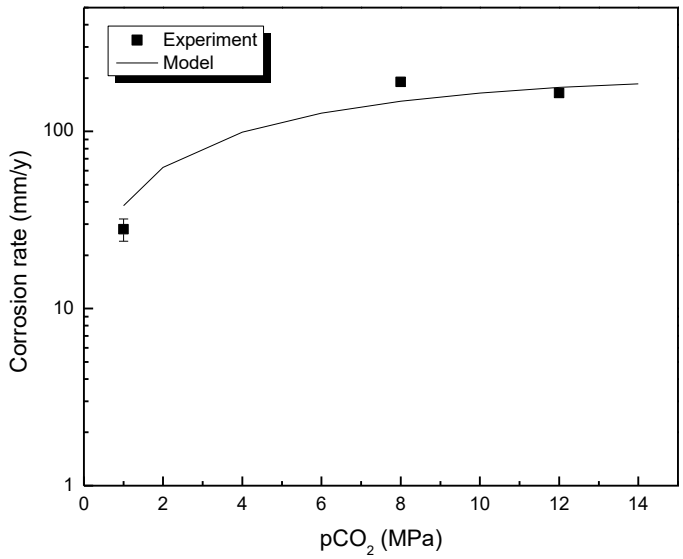

(c)

Figure 10: Comparison of corrosion rates between experiments and predictions in CO_2 environments at different conditions: (a) 0.3 ~ 2 MPa CO_2, 60°C, pH 5, (b) 8 MPa CO_2, 25°C ~ 80°C, pH 3.1 ~ 3.2, (c) 1 MPa ~ 14 MPa CO_2, 80°C, pH 3.1 ~ 3.4.

CONCLUSIONS

A predictive model was developed for corrosion of carbon steel in high pCO_2 conditions by modifying the existing CO_2 corrosion model for low pCO_2. The following conclusions are drawn:

- Water chemistry model was changed by considering non-ideality of the CO_2 phase.
- Electrochemical model was updated by including the Langmuir adsorption isotherm for H_2CO_3.
- $FeCO_3$ formation and growth model was improved by implementing front tracking scheme and exact analytical solution in order to avoid numerical instability.
- Corrosion rates predicted by the updated model showed a good agreement with experimental data under various high pCO_2 conditions.

REFERENCES

1. S. Sim, I. S. Cole, Y.S. Choi, N. Birbilis, “A Review of the Protection Strategies against Internal Corrosion for the Safe Transport of Supercritical CO_2 via Steel Pipelines for CCS Purposes,” *International Journal of Greenhouse Gas Control* 29 (2014): p. 185.
2. L. Wei, Y. Zhang, X. Pang, K. Gao, “Corrosion Behaviors of Steels under Supercritical CO_2 Conditions,” *Corrosion Reviews* 33 (2015): p. 151.
3. S. Sarrade, D. Feron, F. Rouillard, S. Perrin, R. Robin, J.C. Ruiz, H.A. Turc, “Overview on Corrosion in Supercritical Fluids,” *Journal of Supercritical Fluids* 120 (2017): p. 335.
4. Y. Xiang, M. Xu, Y.S. Choi, “State-of-the-Art Overview of Pipeline Steel Corrosion in Impure Dense CO_2 for CCS Transportation: Mechanisms and Models,” *Corrosion Engineering, Science and Technology* 52 (2017): 485.
5. R. Barker, Y. Hua, A. Neville, “Internal Corrosion of Carbon Steel Pipelines for Dense-Phase CO_2 Transport in Carbon Capture and Storage (CCS) - A Review,” *International Materials Reviews* 62 (2017): p. 1.
6. Y. Zhang, K. Gao, G. Schmitt, R.H. Hausler, “Modeling Steel Corrosion under Supercritical CO_2 Conditions,” *Materials and Corrosion* 64 (2013): p. 478.

7. Y. Xiang, Z. Wang, M. Xu, Z. Li, W. Ni, “A Mechanistic Model for Pipeline Steel Corrosion in Supercritical CO_2-SO_2-O_2-H_2O Environments,” *J. of Supercritical Fluids* 82 (2013): p. 1.
8. M.H. Abbas, R. Norman, A. Charles, “Neural Network Modeling of High Pressure CO_2 Corrosion in Pipeline Steels,” *Process Safety and Environmental Protection* 119 (2018): p. 36.
9. R. Nyborg, “CO_2 Corrosion Models for Oil and Gas Production Systems,” CORROSION 2010, paper no. 10371 (Houston, TX: NACE, 2011).
10. M. Seiersten, “Material Selection for Separation, Transportation and Disposal of CO_2,” CORROSION 2001, paper no. 01042 (Houston, TX: NACE, 2001).
11. S. Nesic, M. Nordsveen, R. Nyborg, A. Stangeland, “A Mechanistic Model for CO_2 Corrosion with Protective Iron Carbonate Films,” CORROSION 2001, paper no. 01040 (Houston, TX: NACE, 2001).
12. A.M.K. Halvorsen, T. Sntvedt, “CO_2 Corrosion Model for Carbon Steel including a Wall Shear Stress Model for Multiphase Flow and Limits for Production Rate to Avoid Mesa Attack,” CORROSION 99, paper no. 42 (Houston, TX: NACE, 1999).
13. Y. Zhang, X. Pang, S. Qu, X. Li, K. Gao, “Discussion of the CO_2 Corrosion Mechanism Between Low Partial Pressure and Supercritical Condition,” *Corrosion Science* 59 (2012): p. 186.
14. Y.S. Choi, S. Nesic, “Determining the Corrosive Potential of CO_2 Transport Pipeline in High pCO_2–Water Environments,” *International Journal of Greenhouse Gas Control 5* (2011): p. 788.
15. M. Nordsveen, S. Nesic, R. Nyborg, A. Stangeland, “A Mechanistic Model for Carbon Dioxide Corrosion of Mild Steel in the Presence of Protective Iron Carbonate Films—Part 1: Theory and Verification,” Corrosion 59 (2003): p. 443.
16. S. Nesic, M. Nordsveen, R. Nyborg, A. Stangeland, “A Mechanistic Model for Carbon Dioxide Corrosion of Mild Steel in the Presence of Protective Iron Carbonate Films—Part 2: A Numerical Experiment,” Corrosion 59 (2003): p. 489.
17. S. Nesic, K.-L.J. Lee, “A Mechanistic Model for Carbon Dioxide Corrosion of Mild Steel in the Presence of Protective Iron Carbonate Films—Part 3: Film Growth Model,” Corrosion 59 (2003): p. 616.
18. A. Kahyarian, M. Achour, S. Nesic, “Mathematical Modeling of Uniform CO_2 Corrosion,” *Trends in Oil and Gas Corrosion Research and Technologies*, 1st ed., (Duxford, UK: Woodhead Publishing, 2017), p. 807.
19. N. Spycher, K. Pruess, J. E. King, “CO_2-H_2O Mixtures in the Geological Sequestration of CO_2. I. Assessment and Calculation of Mutual Solubilities from 12 to 100°C and up to 600 bar,” Geochimica et Cosmochimica Acta 67 (2003): p. 3015
20. Z. Duan, R. Sun, “An Improved Model Calculating CO_2 Solubility in Pure Water and Aqueous NaCl Solutions from 273 to 533 K and from 0 to 2000 bar,” Chemical Geology 193 (2003): p. 257.
21. Z. Duan, R. Sun, C. Zhu, I.M. Chou, “An Improved Model for the Calculation of CO_2 Solubility in Aqueous Solutions Containing Na^+, K^+, Ca^{2+}, Mg^{2+}, Cl^-, and SO_4^{2-},” Marine Chemistry 98 (2006): p. 131.
22. M.F. Mohamed, A.M. Nor, M.F. Suhor, M. Singer, Y.S. Choi, S. Nesic, “Water Chemistry for Corrosion Prediction in High Pressure CO_2 Environments,” CORROSION 2011, paper no. 11375 (Houston, TX: NACE, 2011).
23. D. Li, Z. Duan, “The Speciation Equilibrium Coupling with Phase Equilibrium in the H_2O–CO_2–NaCl System from 0 to 250 °C, from 0 to 1000 bar, and from 0 to 5 Molality of NaCl,” Chemical Geology 244 (2007): p. 730.
24. Z. Duan, D. Li, “Coupled Phase and Aqueous Species Equilibrium of the H_2O–CO_2–NaCl–$CaCO_3$ System from 0 to 250°C, 1 to 1000 bar with NaCl Concentrations up to Saturation of Halite,” Geochimica et Cosmochimica Acta 72 (2008): p. 5128.
25. S. Wang, K. George, S. Nesic, “High Pressure CO_2 Corrosion Electrochemistry and the Effect of Acetic Acid,” CORROSION 2004, paper no. 04375 (Houston, TX: NACE, 2011).
26. A.M. Nor, M.F. Suhor, M.F. Mohamed, M. Singer, S. Nesic, "Corrosion of Carbon Steel in High CO_2 Environment: Flow Effect," CORROSION 2011, paper no. 11245 (Houston, TX: NACE, 2011).
27. A.M. Nor, M.F. Suhor, M.F. Mohamed, M. Singer, S. Nesic, “Corrosion of Carbon Steel in High CO_2 Containing Environments: the Effect of High Flow Rate,” CORROSION 2012, paper no. 0001683 (Houston, TX: NACE, 2012).